

Voltage Stability Constrained Economic Dispatch For Multi-Infeed HVDC Power Systems

Jiaxin Wang, *Student Member, IEEE*, Qingchun Hou, *Member, IEEE*, Zhenyu Zhuo, *Member, IEEE*,
Hongyang Jia, *Student Member, IEEE*, and Ning Zhang, *Senior Member, IEEE*

Abstract—Multi-infeed LCC-HVDC decreases voltage stability margins due to its current source nature. Moreover, the high penetration of variable renewable energy makes it difficult to reserve enough margins for all periods. Therefore, voltage stability constraints need to be considered in the scheduling stage. However, the challenge is that the voltage stability margin is not analytic with respect to state variables. We propose a sparse support vector machine to extract the nonlinear voltage stability rule. To embed the rule into economic dispatch (ED), we apply a convex reformulating technique to the rule and then formulate a voltage stability constrained ED (VSCED) model by semi-definite programming. The model is tested on a modified IEEE-14 system and a real-world system from Jiangsu Province, China; and it is compared with other typical data-driven-based models in the Jiangsu system. The numerical experiments suggest that the stability margins can be effectively reserved above the required threshold within an acceptable computation time by the proposed VSCED model, which outperforms the other models.

Index Terms—system scheduling, voltage stability, LCC-HVDC, sparse support vector machine, nonlinear security rule.

NOMENCLATURE

Abbreviations

AC	Alternating Current
DC	Direct Current
HVDC	High Voltage Direct Current
LCC-HVDC	Line-commutated Converter HVDC
CP-CEA	Constant Power Constant Extinction Angle
VRE	Variable Renewable Energy
CPF	Continuous Power Flow
ED	Economic Dispatch
VSCED	Voltage Stability Constrained Economic Dispatch
(S-)SVM	(Sparse) Support Vector Machine
DT	Decision Tree
MLP	Multilayer Perceptron (A Typical Neural Network)
LP	Linear Programming
MILP	Mixed Integer Linear Programming
SDP	Semi-definite Programming

Manuscript received 21 June 2022; revised 8 January 2023 and 29 March 2023; accepted 7 May 2023. This work was supported by the National Key Research and Development Program of China under Grant 2022YFB2403300. Paper no. TPWRS-00915-2022. (Corresponding author: Ning Zhang.)

The authors are with the State Key Laboratory of Power Systems, Department of Electrical Engineering, Tsinghua University, Beijing 100084, China. (email: jiaxinwangthu@gmail.com; ningzhang@tsinghua.edu.cn).

Digital Object Identifier 10.1109/TPWRS.2023.3277213

SOCP	Second Order Cone Programming
<i>Sets</i>	
\mathbb{R}^n	Set of n -dim real (column) vectors
\mathbb{S}^n	Set of $n \times n$ real symmetric matrices
\mathcal{T}	Set of time horizons
\mathcal{E}	Set of edges (branches)
\mathcal{N}_R	Set of buses with VRE
<i>Math Operators</i>	
$\text{diag}(\cdot)$	Map a vector to its corresponding diagonal matrix
$\text{msv}(\cdot)$	Map a matrix to its minimum singular value
$\text{tr}(\cdot)$	Trace of a square matrix
$\langle \cdot, \cdot \rangle$	Euclidean inner product of two matrices
$\ \cdot\ _1, \ \cdot\ _2$	1-norm/2-norm of a vector (or matrix)
$\cdot \geq *, \cdot \leq *$	Element-wise relationship for vectors or scalars
$\cdot \succeq 0$	In semi-definite matrices
$\cdot := *$	Define \cdot by *
<i>Variables</i>	
$P_{\text{ac}}, Q_{\text{ac}}, S_{\text{ac}}$	Vector of AC part active/reactive/complex power injections
$P_{\text{dc}}, Q_{\text{dc}}, S_{\text{dc}}$	Vector of DC part active/reactive/complex power injections
θ, V	Vector of voltage angles/amplitudes
$J, J_{\text{ac}}, J_{\text{dc}}$	Power flow Jacobian matrix and its AC/DC part
$J', J'_{\text{ac}}, J'_{\text{dc}}$	Practical power flow Jacobian matrix and its AC/DC part
ω	Angular frequency
$B_{c,i}$	Compensation susceptance at i th inverter-end bus
X_i	Commutation reactance of i th HVDC
c	Cost vector of generators (and HVDC terminals)

\mathbf{g}_t	Vector of the power generated at time t
\mathbf{d}_t	Vector of nodal load at time t
$\bar{\theta}, \underline{\theta}$	Upper/Lower bounds of voltage angle vectors
$\bar{\mathbf{g}}, \underline{\mathbf{g}}$	Upper/Lower bounds of nodal power generation vectors
$\bar{\mathbf{r}}, \underline{\mathbf{r}}$	Ramping up/down vectors
\bar{P}_{ij}	Transmission capacity of (i, j) branch
$s(\cdot), \tilde{s}(\cdot)$	Real/Fitted stability rule function with respect to power system state variables
$\phi(\cdot)$	Kernel function of SVM
ω, ξ, b	Parameters to be fitted in SVM

I. INTRODUCTION

THE growing requirement for transmitting electricity over a long distance increases the number of invested HVDC lines in power systems. As a result, HVDC lines change the voltage instability mode of the power system. In traditional power systems, voltage collapse only occurs when the load grows to a critical level. However, in multi-infeed HVDC power systems, voltage collapse can also occur when the power transmitted from HVDC reaches to a critical level [1]. Meanwhile, voltage instability may lead to HVDC commutation failure or block fault. For example, on November 12, 2021, a 1000 kV line of East China Power Grid tripped, resulting in seven HVDC commutation failures under insufficient voltage stability margin, and the total power fluctuation exceeded 10 GW [2]. Additionally, the intermittent nature of variable renewable energy (VRE) further reduces the voltage stability margin and makes the stability boundary more complex [3], [4]. Therefore, it is necessary to consider voltage stability margin in the scheduling stage.

A typical scheduling technique considering voltage stability margin is voltage stability constrained economic dispatch (VSCED). There are several relevant studies on economic dispatch (ED) considering voltage stability margins [5]–[8]. Most studies follow a similar two-step pattern: 1) extracting the voltage stability rule and 2) embedding the rule into ED. The extracting step approximates the relationship between voltage stability margin and power system state variables, and then obtains a voltage stability rule. However, the rule may be unsuitable to be directly treated as a constraint in optimizations. Thus, the next step is required to reformulate the extracted rule. Moreover, the relationship between the voltage stability margin and power system state variables is complicated and non-analytic [9], [10]. It is thus hard to consider voltage stability in ED. Researchers have developed model-driven and data-driven methods to cope with the problem [11].

Model-driven methods seek explicit sufficient conditions for voltage stability to formulate a convex VSSED model [12]. Plenty of techniques have been developed in the last few years. Firstly, heuristic voltage stability indices, such as L -index [13], and continuous power flow (CPF) index [14], have been considered in VSSED. The square-sum of L -index has been embedded into the objective, and the model has been solved by a trust region method [15]. The maximum of the L -index average has been embedded into the constraints, and the

model has been solved by a genetic algorithm [16]. Then, the CPF index has been embedded into the constraints for market-clearing [17]. The heuristic voltage stability indices are easily considered in ED for their simple mathematical structures. However, those indices might be invalid under power systems with high penetration of VRE. To tackle the diverse operation patterns caused by VRE, researchers have developed VSSED based on power flow Jacobian. The singularity of power flow Jacobian implies voltage collapse. A sufficient condition for the nonsingularity of power flow Jacobian has been found [18] and has been embedded into optimal power flow as second-order cone programming (SOCP) [19]. The minimum singular value of power flow Jacobian is considered a voltage stability margin in optimal power flow, formulating a semi-definite programming (SDP) problem [5]. The Jacobian-based methods usually reserve a lower bound for voltage stability margin. However, they may find it difficult to consider the influence of HVDC terminals. New sufficient conditions are required but still hard to be found. Therefore, plenty of data-driven methods have been developed recently to cope with the problem.

Data-driven methods fit voltage stability boundaries via suitable mathematical structures [20]. Some data-driven methods focus on assessing voltage stability. Researchers have taken full advantage of the precision and generalization of those methods. A graph neural network has been applied to assess the real-time voltage stability [21]. A bidirectional long short term memory network has been applied to monitor the voltage stability of hybrid AC/DC microgrids [22]. A two-stage Bayes inference has been applied to evaluate the joint voltage stability simultaneously [23]. Such methods have shown a great ability to assess the voltage stability given operation states, but the assessment models are usually difficult to be embedded. Then, researchers have explored several linear or half-linear (piecewise linear) data-driven methods to embed stability rules into optimizations. A piecewise linear regression model based on least square approximation has been applied to embed the stability constraint into system scheduling [24] and unit commitment [25]. A decision tree (DT) model has been applied [26] and has been further improved with the sparse technique and the ensemble technique [27]. A multilayer perceptron (MLP) has been piece wisely linearized to approximate the stability constraint in small-scale systems [28], [29]. Those methods have taken advantage of the piecewise linearization techniques in optimization modeling.

However, there are still three main issues to be addressed. First, HVDC terminals complicate the voltage instability pattern. The voltage stability boundary becomes more complex after considering HVDC terminals since it introduces a nonlinear term in power flow Jacobian [1]. A model with a nonlinear structure is then required to fit the voltage stability boundary with high accuracy. Second, the complexity of solving mixed integer programming grows rapidly as the number of binary decision variables increases. Then the extracted voltage stability rule is expected to introduce as few binary decision variables as possible (even introducing no binary decision variable). Third, the voltage stability problem often shows a sparse characteristic. The number of principal factors is relatively small compared with the number of system state

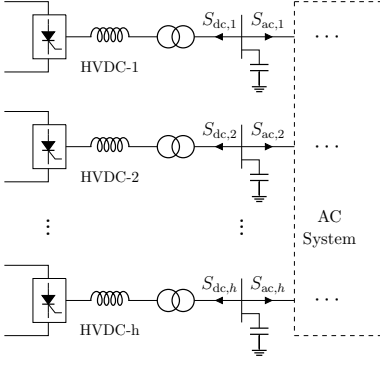


Fig. 1. Multi-infeed HVDC power system.

variables [19], [30], [31]. The extracted voltage stability rule is thus required to be sparse.

Here, we propose methods to formulate VSced considering HVDC terminals to fill the gap. Firstly, we propose a sparse support vector machine (S-SVM) model to extract the voltage stability boundary and extracts a sparse nonlinear rule. Then we relax the rule and reformulate it into SDP constraints without introducing binary decision variables. Finally, we formulate the whole VSced as SDP and test it on a modified IEEE-14 system and a real-world system from Jiangsu Province, China. Other typical data-driven methods, decision tree (DT) and multilayer perceptron (MLP), are also compared.

The contribution of this paper is twofold:

- 1) We propose an S-SVM to extract the nonlinear voltage stability rules.
- 2) We formulate a VSced model considering the influence of multi-infeed HVDC terminals without introducing binary decision variables.

The remainder of this paper is organized as follows. Section II describes the mechanism of voltage stability considering HVDC terminals. Section III proposes the S-SVM method to extract the voltage stability rule and then reformulates and embeds the rule into ED to build the VSced model. Section IV validates the proposed VSced model by a modified IEEE-14 system and a real-world system from Jiangsu Province, China. Section V concludes this paper.

II. PROBLEM FORMULATION

A. Voltage Stability Analysis Considering HVDC Terminals

This subsection derives the voltage stability index based on the power flow Jacobian matrix. A multi-infeed HVDC power system in steady states is considered in our study. The n -bus system is illustrated as Fig. 1, and only buses connected with the h HVDC terminals are drawn explicitly ($h \leq n$). Here HVDC is modeled as line-commutated converters (LCC) under constant power constant extinction angle (CP-CEA) control mode, and in Section II-B, the HVDC is modeled as an inverter-based generator in the optimization problems. It should be noted that the proposed method in this paper is effective irrespective of HVDC control modes. Although different HVDC control modes may result in different values of

the stability margin, the proposed method can extract different voltage stability rules under different control modes and then embeds the proper rule into the optimization (or embeds all rules into the optimization to get a robust scheduling result). The reference directions of the complex power S_{ac} and S_{dc} are labeled in Fig. 1 respectively, and $S_{ac} = P_{ac} + iQ_{ac}$, $S_{dc} = P_{dc} + iQ_{dc}$. For LCC under such control mode, the active power P_{dc} and reactive power Q_{dc} injected into the inverter-end AC bus only depend on its voltage phasor (both amplitude and angle) [1]. Thus, system power flow is expressed as

$$\mathbf{f}(\boldsymbol{\theta}, \mathbf{V}) := \begin{bmatrix} \mathbf{P}^{SP} - \mathbf{P}_{ac}(\boldsymbol{\theta}, \mathbf{V}) - \mathbf{P}_{dc}(\boldsymbol{\theta}, \mathbf{V}) \\ \mathbf{Q}^{SP} - \mathbf{Q}_{ac}(\boldsymbol{\theta}, \mathbf{V}) - \mathbf{Q}_{dc}(\boldsymbol{\theta}, \mathbf{V}) \end{bmatrix} = 0. \quad (1)$$

where $\mathbf{f}(\boldsymbol{\theta}, \mathbf{V}) = 0$ denotes power flow equations. $\boldsymbol{\theta}$ and \mathbf{V} are voltage angle vector and voltage amplitude vector respectively. \mathbf{P}^{SP} and \mathbf{Q}^{SP} are specified nodal power injections. $\mathbf{P}_{ac}(\boldsymbol{\theta}, \mathbf{V})$ and $\mathbf{Q}_{ac}(\boldsymbol{\theta}, \mathbf{V})$ represent AC part power flow; $\mathbf{P}_{dc}(\boldsymbol{\theta}, \mathbf{V})$ and $\mathbf{Q}_{dc}(\boldsymbol{\theta}, \mathbf{V})$ represent DC part power flow.

Voltage instability is related to the singularity of power flow Jacobian matrix J defined as (2). The whole system Jacobian matrix J can be divided into AC part J_{ac} and DC part J_{dc} respectively.

$$J := \left[\frac{\partial \mathbf{f}}{\partial \boldsymbol{\theta}^T}, \frac{\partial \mathbf{f}}{\partial \mathbf{V}^T} \right] = J_{ac} + J_{dc}. \quad (2)$$

$$J_{ac} = - \begin{bmatrix} \frac{\partial \mathbf{P}_{ac}}{\partial \boldsymbol{\theta}^T} & \frac{\partial \mathbf{P}_{ac}}{\partial \mathbf{V}^T} \\ \frac{\partial \mathbf{Q}_{ac}}{\partial \boldsymbol{\theta}^T} & \frac{\partial \mathbf{Q}_{ac}}{\partial \mathbf{V}^T} \end{bmatrix},$$

$$J_{dc} = - \begin{bmatrix} \frac{\partial \mathbf{P}_{dc}}{\partial \boldsymbol{\theta}^T} & \frac{\partial \mathbf{P}_{dc}}{\partial \mathbf{V}^T} \\ \frac{\partial \mathbf{Q}_{dc}}{\partial \boldsymbol{\theta}^T} & \frac{\partial \mathbf{Q}_{dc}}{\partial \mathbf{V}^T} \end{bmatrix}. \quad (3)$$

According to characteristics of LCC under CP-CEA control mode, both \mathbf{P}_{dc} and \mathbf{Q}_{dc} are irrelevant to the phase angle $\boldsymbol{\theta}$. DC power injected from HVDC terminals is almost decoupled from the voltage amplitude [32]. Then

$$\frac{\partial \mathbf{P}_{dc}}{\partial \boldsymbol{\theta}^T} \approx 0, \frac{\partial \mathbf{Q}_{dc}}{\partial \boldsymbol{\theta}^T} \approx 0, \frac{\partial \mathbf{P}_{dc}}{\partial \mathbf{V}^T} \approx 0. \quad (4)$$

The only nonzero block in J_{dc} is calculated according to [1], [32].

$$\frac{\partial \mathbf{Q}_{dc}}{\partial \mathbf{V}^T} = \text{diag} \left(\frac{2c_i K(c_i) P_{dc,i}}{V_i} + 2\omega B_{c,i} V_i \right), \quad (5)$$

where $P_{dc,i}$ is the active HVDC power injected at the i th inverter-end bus, ω is the angular frequency, $B_{c,i}$ is the reactive power compensation capacitor at i th inverter-end bus. c_i and $K(c_i)$ are as

$$c_i := \frac{X_i I_{d,i}}{\sqrt{2} K_i V_i},$$

$$K(c_i) := \frac{1}{(\cos \gamma_i - c_i)^2 \sqrt{1 - (\cos \gamma_i - c_i)^2}}, \quad (6)$$

where X_i is the commutation reactance of i th HVDC. γ_i is the extinction angle of i th inverter. K_i is the ratio of the transformer of i th HVDC. $I_{d,i}$ is the DC current flowing through i th HVDC. For convenience, power flow is rewritten

by (7), where J' denotes the corresponding Jacobian. Then the Jacobian is calculated by (8).

$$\begin{bmatrix} \Delta P/V \\ \Delta Q/V \end{bmatrix} = -J' \begin{bmatrix} V \Delta \theta \\ \Delta V \end{bmatrix}, \quad (7)$$

$$J' \approx J'_{ac} + \begin{bmatrix} 0 & 0 \\ 0 & \text{diag}\left(\frac{2c_i K(c_i) P_{dc,i}}{V_i^2} + 2\omega B_{c,i}\right) \end{bmatrix}. \quad (8)$$

The voltage collapses when J' becomes singular [1]. Thus, the minimum singular value of J' is a suitable measurement for voltage stability margins. The following theorem describes this correspondence more precisely [33].

Theorem 1. For nonsingular matrix A ,

$$\min\{\|\Delta A\|_2 \mid A + \Delta A \text{ is singular}\} = \text{msv}(A), \quad (9)$$

i.e., the minimum singular value of a matrix is the distance between the matrix and the set consisting of all the singular matrices.

Proof. If $\|A^{-1}\|_2 \|\Delta A\|_2 < 1$, then $\|A^{-1} \Delta A\|_2 \leq \|A^{-1}\|_2 \|\Delta A\|_2 < 1$, we see $I + A^{-1} \Delta A$ is nonsingular, and thus $A + \Delta A$ is nonsingular. Therefore,

$$\min\{\|\Delta A\|_2 \mid A + \Delta A \text{ is singular}\} \geq \frac{1}{\|A^{-1}\|_2}. \quad (10)$$

On the other hand, since $\|\cdot\|_2$ is an operator norm, there exists x with $\|x\|_2 = 1$ such that $\|A^{-1}x\|_2 = \|A^{-1}\|_2$. Choosing

$$y = \frac{A^{-1}x}{\|A^{-1}x\|_2}, \quad \Delta A = -\frac{xy^T}{\|A^{-1}\|_2}, \quad (11)$$

gives $(A + \Delta A)y = 0$, $\|\Delta A\|_2 = \frac{1}{\|A^{-1}\|_2}$, which implies the inequality can hold, i.e.,

$$\min\{\|\Delta A\|_2 \mid A + \Delta A \text{ is singular}\} = \frac{1}{\|A^{-1}\|_2}. \quad (12)$$

Finally, denote the singular values of A by $\sigma_1 \geq \sigma_2 \geq \dots \geq \sigma_{n-1} \geq \sigma_n > 0$, then the singular values of A^{-1} are $\frac{1}{\sigma_n} \geq \frac{1}{\sigma_{n-1}} \geq \dots \geq \frac{1}{\sigma_2} \geq \frac{1}{\sigma_1} > 0$. Since the matrix 2-norm is equal to the maximum singular value of the matrix, we see $\|A^{-1}\|_2 = \frac{1}{\sigma_1}$, which implies

$$\min\{\|\Delta A\|_2 \mid A + \Delta A \text{ is singular}\} = \sigma_n = \text{msv}(A). \quad (13)$$

□

As analyzed above, the minimum singular value goes down toward zero as the system operation approaches the critical point of voltage collapse. Therefore, a voltage stability rule can be expressed as

$$s(\cdot) = s_0 - \text{msv}(J') \leq 0, \quad (14)$$

where s_0 is the required voltage stability threshold, $\text{msv}(\cdot)$ is the function that maps J' to its minimum singular value, $s(\cdot) \leq 0$ is the criteria for voltage stability.

B. Voltage Stability Constrained Economic Dispatch

This subsection builds the structure of a VSCEP problem, where voltage stability constraints are to be implemented in the next section. The VSCEP model is written as (15), where (15a)-(15h) constitute ED without voltage stability constants, and (15i)-(15j) represents the voltage stability constraints derived from (14). In detail, (15a) represents the objective, where c is the cost vector of generators, and g_t is the power injected from generators and HVDC terminals at time t . (15b) represents the DC power flow equations, where B_0 is the susceptance matrix built by branch susceptance, θ_t is the phase angle vector at time t , and d_t is the load vector at time t . (15c) sets the reference of phase angle. (15d) represents the limits for phase angle, where $\underline{\theta}$ and $\bar{\theta}$ denote the lower bound and the upper bound respectively. (15e) represents the constraint for the predicted outputs of VRE, where $P_{i,t}$ is the predicted output of i th VRE output at time t . (15f) represents the lower and upper bounds for generator outputs, where g and \bar{g} denote corresponding bounds. (15g) represents the limits of branch flow, where X_{ij} denotes the branch reactance, and \bar{P}_{ij} denotes the upper bound. (15h) represents the limits of the ramping capability of generators, where r and \bar{r} denote corresponding bounds. \mathcal{T} , \mathcal{N}_R , \mathcal{E} are sets of periods, VRE bus indices, and branches, respectively.

$$\min_g \sum_{t \in \mathcal{T}} c^T g_t \quad (15a)$$

$$\text{s.t. } B_0 \theta_t = g_t - d_t \quad \forall t \in \mathcal{T} \quad (15b)$$

$$\theta_{n,t} = 0 \quad \forall t \in \mathcal{T} \quad (15c)$$

$$\underline{\theta} \leq \theta_t \leq \bar{\theta} \quad \forall t \in \mathcal{T} \quad (15d)$$

$$g_{i,t} = P_{i,t} \quad \forall i \in \mathcal{N}_R \quad \forall t \in \mathcal{T} \quad (15e)$$

$$g \leq g_t \leq \bar{g} \quad \forall t \in \mathcal{T} \quad (15f)$$

$$\left| \frac{\theta_{i,t} - \theta_{j,t}}{X_{ij}} \right| \leq \bar{P}_{ij} \quad \forall (i,j) \in \mathcal{E} \quad \forall t \in \mathcal{T} \quad (15g)$$

$$r \leq g_{t+1} - g_t \leq \bar{r} \quad \forall t \in \mathcal{T} \quad (15h)$$

$$x_t^T := [g_t^T, \theta_t^T] \quad \forall t \in \mathcal{T} \quad (15i)$$

$$\tilde{s}(x_t) \leq 0 \quad \forall t \in \mathcal{T} \quad (15j)$$

To maintain required voltage stability margins for every optimal operation point, constraint (15j) is embedded. As declared above, $s(\cdot)$ denotes the real classifier function of voltage stability under a certain threshold. The abstract function $\tilde{s}(\cdot)$ thus denotes the extracted voltage stability rule which is the approximation of the real $s(\cdot)$. In section III, we will furthermore implement the approximate form.

III. VOLTAGE STABILITY RULE EXTRACTION AND EMBEDDING

A. Framework

The framework for modeling VSCEP is shown in Fig. 2. First, we prepare the dataset on operation states. We take full advantage of the boundary conditions of ED to reduce the sample space in III-B. Based on the reduced sample space, we obtain the dataset on operation states and evaluate the voltage

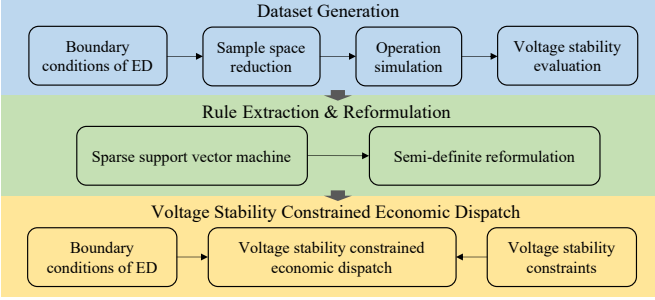


Fig. 2. Framework for modeling voltage stability constrained economic dispatch considering HVDC terminals.

stability by (14). Second, we propose a sparse support vector machine (S-SVM) to extract the voltage stability rule in III-C. Then we relax the extracted rule into a semi-definite constraint and embed it into ED in III-D. Finally, a VSCED model is formulated as SDP, and the required voltage stability margin is reserved in the scheduling results.

B. Sample Space Reduction

This subsection reduces the sample space based on the boundary conditions of ED. It should be noted that the sample space reduction can be skipped if a full dataset has been already obtained (e.g., a full historical dataset has been given), on which the proposed extracting and embedding methods still keep valid.

The dimension of the sample space is the same as the number of system state variables. Although the state variables can be chosen differently, the number is always $2n - 1$ for an n -bus system. Suppose an n -bus system with k sampled values per dimension, the total number of operation points to be sampled is up to $\mathcal{O}(k^{2n-1})$, which grows exponentially with respect to the size of the power system.

Boundary conditions of optimizations can reduce the sample space. As for deterministic ED, the load forecasting results are considered a pre-known condition, i.e., the load condition is fixed before solving ED. Thus, only buses with generators or HVDC terminals contribute a freedom degree to the whole sample space. Denote the number of these buses by m , and the size of the dataset to be sampled is reduced to $\mathcal{O}(k^{2m-1})$. (16) shows the difference between the two sampling methods, where \mathbf{x} is the free state variable under certain boundary conditions; \mathbf{p} is the fixed state variable under the boundary conditions. The voltage stability rule extracted from the original sample space is left-hand side. In contrast, the right-hand side is the voltage stability rule extracted from the reduced sample space, whose calculation burden is also reduced. We would like to clarify that the sample space reduction will not have any additional negative impact on the optimization results. The only possible error lies in the differences between the load forecasting results and the actual load injections, which exceeds the scope of ED.

$$\tilde{s}(\mathbf{x}; \mathbf{p}) \Rightarrow \tilde{s}_{\mathbf{p}}(\mathbf{x}). \quad (16)$$

Based on the reduced sample space, the modified Latin hypercube sampling (LHS) method [34] is applied to sample the

output of generators and HVDC terminals to obtain operation states \mathbf{x} . Although other sampling methods [35], [36] proposed in recent years can also be applied to the reduced sample space without obstacles, it is not the focus of this paper.

Then we label the operation states using (14) by $y \in \{-1, 1\}$, where $y = 1$ indicates that the operation state is facing a voltage stability issue and vice versa. Finally, the dataset \mathcal{D} is generated as

$$\mathcal{D} := \{\mathbf{x}; y\}. \quad (17)$$

Without ambiguity, we write $\tilde{s}(\cdot)$ instead of $\tilde{s}_{\mathbf{p}}(\cdot)$ to represent the voltage stability rule extracted from the reduced sample space in later paragraphs for convenience.

C. Extracting The Rule By Sparse Support Vector Machine

This subsection proposes a sparse support vector machine (S-SVM) to extract the sparse and nonlinear voltage stability rule. The nonlinear nature of the voltage stability rule has been shown in (8)-(14). The voltage stability rule thus can be formulated as a nonlinear binary classifier statistically, given a required voltage stability margin threshold. Therefore, we propose a sparse support vector machine to extract the sparse and nonlinear voltage stability rule. The proposed S-SVM is developed based on SVM, formulated as (18).

$$\min_{\omega, b, \xi} \frac{1}{2} \|\omega\|_2^2 + \frac{C}{n} \sum_{i=1}^n \xi_i \quad (18a)$$

$$\text{s.t. } y_i(\omega^T \phi(\mathbf{x}_i) + b) \geq 1 - \xi_i \\ \xi_i \geq 0, \quad 1 \leq i \leq n \quad (18b)$$

where $(\mathbf{x}_i, y_i) \in \mathcal{D}$ is the i th labeled sample in dataset \mathcal{D} , $\phi(\cdot)$ denotes a nonlinear basis function which is preassigned, C is a hyperparameter which controls the weight, and ω, b, ξ denotes the SVM parameters to be solved. (18a) maximizes the gap between the stable and unstable parts. It also introduces a penalty term $\frac{C}{n} \sum_{i=1}^n \xi_i$ to allow a soft-margin classification. (18b) represents the constraints for the two classes, and only a few constraints (corresponding to support vectors) are valid.

However, SVM (18) cannot be directly applied to extract the voltage stability rule for VSSED in power systems. We note that the voltage stability rule has some sparsity patterns. The buses that are far away from those heavy-load buses and heavy-power-injected HVDC terminals usually contribute little to the voltage stability. Therefore, a sparse voltage stability rule is required for VSSED in power systems. Then S-SVM is proposed as (19).

$$\min_{\omega, b, \xi} \frac{1}{2} \|\omega\|_1 + \frac{1}{n} \sum_{i=1}^n C_i \xi_i \quad (19a)$$

$$\text{s.t. } y_i(\omega^T \phi(\mathbf{x}_i) + b) \geq 1 - \xi_i \\ \xi_i \geq 0, \quad 1 \leq i \leq n \quad (19b)$$

To ensure the sparsity of the voltage stability rule, 1-norm $\|\cdot\|_1$ is applied on the weight coefficients ω to form the lasso term in objective (19a). On the one hand, the non-differentiable at zeros ensures that the lasso term

can eliminate noise features by estimating their coefficients by zero. On the other hand, the lasso term keeps the convexity of the whole S-SVM model such that the voltage stability rule can still be extracted efficiently. Moreover, S-SVM can also ensure certain robustness for the voltage stability rule. The coefficients C_i of the soft-margin variable ξ_i is an adjustable hyperparameter. Different C_i can be chosen differently according to the corresponding sample i . For those important samples whose voltage stability margins are severely small, the corresponding coefficients C_i should be relatively large. Such a simple principle makes it robust for the extracted voltage stability rule.

Note that although the lasso term is non-differentiable at zero, it is still a convex function with respect to ω [37]. Therefore, S-SVM (19) keeps a convex optimization problem. Besides, the lasso term has a well-defined sub-gradient, which means S-SVM (19) can still be solved using the Stochastic Gradient Descent (SGD) method same as the original SVM (18).

D. Embedding The Rule By Semi-definite Programming

This subsection applies an SDP relaxation on the extracted voltage stability rule and embeds the rule into ED to formulate a VSSED model. The rule extracted by S-SVM needs reformulating to be embedded in VSSED for its nonlinearity. However, piecewise linearization techniques are not suitable since such techniques would introduce extra binary decision variables in ED. Therefore, there is a trade-off when selecting a suitable basis function. This paper uses the quadratic basis function to model the VSSED problem for its nonlinearity and simplicity. Here the basis function $\phi(\cdot)$ is a mapping from \mathbb{R}^d to $\mathbb{R}^{\frac{(d+1)(d+2)}{2}}$ as (20).

$$\begin{aligned} \phi : \quad \mathbb{R}^d &\longrightarrow \mathbb{R}^{\frac{(d+1)(d+2)}{2}} \\ (x_i)_{i=1}^d &\longmapsto [(a_{ij}x_i x_j)_{i,j=1}^d, (a_i x_i)_{i=1}^d, a_0] \end{aligned} \quad (20)$$

where $(x_i)_{i=1}^d$ means a d -dim vector whose elements are x_1, x_2, \dots, x_d respectively, $(x_i x_j)_{i,j=1}^d$ means a $d(d+1)/2$ -dim vector whose elements are $x_1^2, x_1 x_2, \dots, x_1 x_d, x_2^2, x_2 x_3, \dots, x_d^2$ respectively, a_{ij}, a_i are all preassigned parameters, and $[\cdot, \cdot]$ concatenates two vectors to form a new vector.

With the basis function (20), the voltage stability rule is then implemented as

$$\begin{aligned} \tilde{s}(\mathbf{x}) &= \omega^T \phi(\mathbf{x}) + b \\ &= \mathbf{x}^T A \mathbf{x} + \mathbf{a}^T \mathbf{x} + r, \end{aligned} \quad (21)$$

where $A \in \mathbb{S}^d$ is a real symmetric square matrix, $\mathbf{a} \in \mathbb{R}^d$ is a real vector, and $r \in \mathbb{R}$ is a real number. $\tilde{s}(\mathbf{x}) \leq 0$ represents that the voltage stability margin is above the required margin and vice versa. Then constraint (15j) is implemented by (21) as

$$F = \{\mathbf{x} \in \mathbb{R}^d \mid \mathbf{x}^T A \mathbf{x} + \mathbf{a}^T \mathbf{x} + r \leq 0\}. \quad (22)$$

However, (22) is nonconvex if quadratic form matrix A is indefinite. Thus (22) is unsuitable to be embedded directly into ED (15). We note that the nonconvexity only concentrates on the quadratic part $\mathbf{x}^T A \mathbf{x}$, and that $\mathbf{x}^T A \mathbf{x} = \langle A, \mathbf{x} \mathbf{x}^T \rangle$ is an identity transformation where $\langle A, X \rangle := \text{tr}(A^T X)$ is the trace

of $A^T X$. Then we can convert the nonconvex part into a linear part by introducing a new symmetric matrix decision variable $X \in \mathbb{S}^d$ (\mathbb{S}^d denotes the $d \times d$ symmetric matrix space). The nonconvexity is thus transformed into $X = \mathbf{x} \mathbf{x}^T$ constraint as (23).

$$\left\{ (\mathbf{x}, X) \in \mathbb{R}^d \times \mathbb{S}^d \mid \begin{array}{l} \langle A, X \rangle + \mathbf{a}^T \mathbf{x} + r \leq 0 \\ X = \mathbf{x} \mathbf{x}^T \end{array} \right\}. \quad (23)$$

We point out that (23) is a rank-one constraint. Then (23) can be relaxed into a semi-definite constraint [38] as

$$\left\{ (\mathbf{x}, X) \in \mathbb{R}^d \times \mathbb{S}^d \mid \begin{array}{l} \langle A, X \rangle + \mathbf{a}^T \mathbf{x} + r \leq 0 \\ \begin{bmatrix} 1 & \mathbf{x}^T \\ \mathbf{x} & X \end{bmatrix} \succeq 0 \end{array} \right\}, \quad (24)$$

where $\succeq 0$ limits the matrix to be positive semi-definite (PSD). Considering the upper and lower boundaries of \mathbf{x} , valid inequalities for X can be added further to tighten (24). Finally, the set of voltage stability constraints can be written as

$$\hat{F} = \left\{ (\mathbf{x}, X) \in \mathbb{R}^d \times \mathbb{S}^d \mid \begin{array}{l} \langle A, X \rangle + \mathbf{a}^T \mathbf{x} + r \leq 0 \\ \begin{bmatrix} 1 & \mathbf{x}^T \\ \mathbf{x} & X \end{bmatrix} \succeq 0 \\ \mathbf{l} \leq \mathbf{x} \leq \mathbf{u} \\ \mathbf{l} \mathbf{x}^T + \mathbf{x} \mathbf{l}^T - \mathbf{l} \mathbf{l}^T \leq X \\ \mathbf{u} \mathbf{x}^T + \mathbf{x} \mathbf{u}^T - \mathbf{u} \mathbf{u}^T \leq X \\ \mathbf{X} \leq \mathbf{x} \mathbf{u}^T + \mathbf{l} \mathbf{x}^T - \mathbf{l} \mathbf{u}^T \\ \mathbf{X} \leq \mathbf{x} \mathbf{l}^T + \mathbf{u} \mathbf{x}^T - \mathbf{u} \mathbf{l}^T \end{array} \right\}, \quad (25)$$

where $\mathbf{l}, \mathbf{u} \in \mathbb{R}^d$ are the lower and the upper boundary of \mathbf{x} respectively.

Based on \hat{F} in (25), a VSSED model is finally formulated as (26).

$$\min_{\mathbf{g}} \sum_{t \in \mathcal{T}} \mathbf{c}^T \mathbf{g}_t \quad (26a)$$

$$\text{s.t. } (15b) - (15h) \quad (26b)$$

$$\mathbf{l}^T := [\underline{\mathbf{g}}^T, \underline{\boldsymbol{\theta}}^T], \mathbf{u}^T := [\bar{\mathbf{g}}^T, \bar{\boldsymbol{\theta}}^T] \quad (26c)$$

$$\mathbf{x}_t^T := [\mathbf{g}_t^T, \boldsymbol{\theta}_t^T] \quad \forall t \in \mathcal{T} \quad (26d)$$

$$\langle A, X_t \rangle + \mathbf{a}^T \mathbf{x}_t + r \leq 0 \quad \forall t \in \mathcal{T} \quad (26e)$$

$$\begin{bmatrix} 1 & \mathbf{x}_t^T \\ \mathbf{x}_t & X_t \end{bmatrix} \succeq 0 \quad \forall t \in \mathcal{T} \quad (26f)$$

$$\mathbf{l} \mathbf{x}_t^T + \mathbf{x}_t \mathbf{l}^T - \mathbf{l} \mathbf{l}^T \leq X_t \quad \forall t \in \mathcal{T} \quad (26g)$$

$$\mathbf{u} \mathbf{x}_t^T + \mathbf{x}_t \mathbf{u}^T - \mathbf{u} \mathbf{u}^T \leq X_t \quad \forall t \in \mathcal{T} \quad (26h)$$

$$X_t \leq \mathbf{x}_t \mathbf{u}^T + \mathbf{l} \mathbf{x}_t^T - \mathbf{l} \mathbf{u}^T \quad \forall t \in \mathcal{T} \quad (26i)$$

$$X_t \leq \mathbf{x}_t \mathbf{l}^T + \mathbf{u} \mathbf{x}_t^T - \mathbf{u} \mathbf{l}^T \quad \forall t \in \mathcal{T} \quad (26j)$$

The SDP problem's time complexity is related to the size of the matrix decision variable X , and the size of X is determined by the sparsity of quadratic form matrix A . If A is a dense matrix, then X must have a $\mathcal{O}(d^2)$ size, which would heavily worsen the time complexity. In contrast, if A is an s -sparse matrix (i.e., A has at most s nonzero columns or rows) where s is far less than d , then X would be reduced into size s , and the

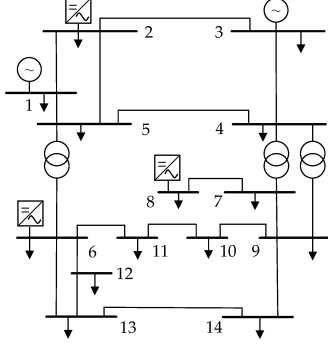


Fig. 3. IEEE-14 network. Three HVDC terminals are set at Bus #2, Bus #6, and Bus #8, respectively.

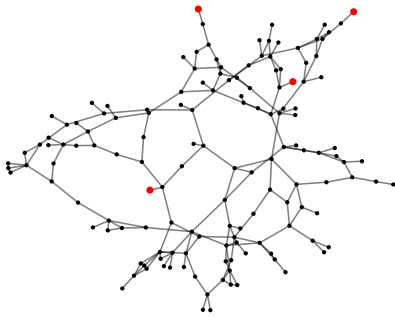


Fig. 4. Jiangsu-2020 topology. Four HVDC terminals are marked in red.

time complexity of the SDP problem is approximately close to that of the linear problem. Therefore, the sparse voltage stability rule theoretically improves the solving efficiency for VSCED.

IV. CASE STUDY

A. Data Description

This section studies two typical cases (IEEE-14, Jiangsu-2020) to validate the proposed VSSED-HVDCT model and corresponding methods. In detail, case IEEE-14 is modified from the standard IEEE 14-bus case. Three HVDC terminals are added at Bus #2, Bus #6, and Bus #8 respectively. In addition, two conventional units are added at Bus #1 and Bus #3. The modified network is shown in Fig. 3. Case Jiangsu-2020 is extracted from a real-world power transmission system of Jiangsu Province, China. Only the buses with voltage levels higher than 500 kV are considered, and the Thevenin equivalence method reduces other buses with lower voltage levels. Since Jiangsu Province relies heavily on outside electric energy transmitted from other provinces through HVDC, validating the proposed methods in such a case is convincing. The network of case Jiangsu-2020 contains 141 buses, 185 branches, 111 equivalent generators, and four ultra HVDC terminals (i.e., JP HVDC, YH HVDC, BH HVDC, and XT HVDC). The peak load is 115000 MW, the total HVDC capacity is 22020 MW, and the penetration of VRE is about 25%. The topology is shown in Fig. 4. Both the two cases consider the period of one day ahead with fifteen minutes intervals (a total of 96 operation points). The rest of this

section is organized as follows. Section IV-B focuses on the understanding and explanation of the extracted rule and the proposed VSSED model based on the IEEE-14 case. Section IV-C focuses on the effect of the extracted rule and the solving time of VSSED based on the Jiangsu-2020 case. Section IV-D compares the proposed method with the other two typical data-driven methods (decision tree and multilayer perceptron). Section IV-E discusses the generalization of VSSED to different load levels. The simulation is finished by MATLAB and Python3 and is solved by MOSEK 9.3 (for SDP) and Gurobi 9.5 (for MILP) on AMD-RT-5900X CPU.

B. Rule Extraction and Explanation

This subsection studies the characteristics of the extracted voltage stability rule based on the IEEE-14 case. Firstly, the method proposed in Section III-B is applied to generate the dataset \mathcal{D} . Fig. 5(a) describes the relationship between voltage stability margin (minimum singular value) and total power injection from HVDC terminals. The relationship shows a general trend that the voltage stability margin decreases as the total power injection from HVDC terminals increases. However, different HVDC terminals may have significantly different influences on voltage stability. Fig. 5(b)-(c) illustrate such a relationship in detail. Fig. 5(b) shows that the HVDC terminals at Bus #6 and Bus #8 have a relatively significant influence on voltage stability, while Fig. 5(c) shows that the HVDC terminal at Bus #2 has little influence on voltage stability. The reason is that the HVDC terminal at Bus #2 is close to voltage sources and far from load buses in the metric of the electrical distance. Moreover, Fig. 5(d) shows the nonlinear characteristics of the voltage stability boundary. Then, the dataset is split into training and test sets. S-SVM (19) is applied to the train set to extract the voltage stability rule. Table I lists the statistic indices for the extraction. The four indices suggest that the model performs well on the test set. The model is accurate and unbiased. An extracted voltage stability rule is given in (27) as an example.

$$-1.42g_1^2 - 4.97g_1 + 8.11g_6 + 23.08g_8 - 0.92 \leq 0, \quad (27)$$

where g_1 is the generator output at Bus #1; g_6 and g_8 are the HVDC outputs at Bus #6 and Bus #8 respectively. The result suggests that 1) The HVDC terminals at Bus #6 and Bus #8 greatly negatively influence the voltage stability. 2) The projection on these two HVDC terminals shows a simple linear relationship, which is consistent with Fig. 5 shown above. 3) The HVDC terminal at Bus #2 has little influence on the voltage stability, which is consistent with the fact that the HVDC terminal is close to voltage sources and is far from load buses in the sense of electrical distance. Fig. 6 shows the scheduling result of generator output, which gives detailed information about how the extracted rule affects the scheduling results. By embedding the voltage stability rule into ED, the voltage stability margin is maintained by limiting the power injected from the HVDC terminal at Bus #8. The system is still balanced under such a limit since other units are scheduled to generate more power. The price for the constraint is a little additional generating cost.

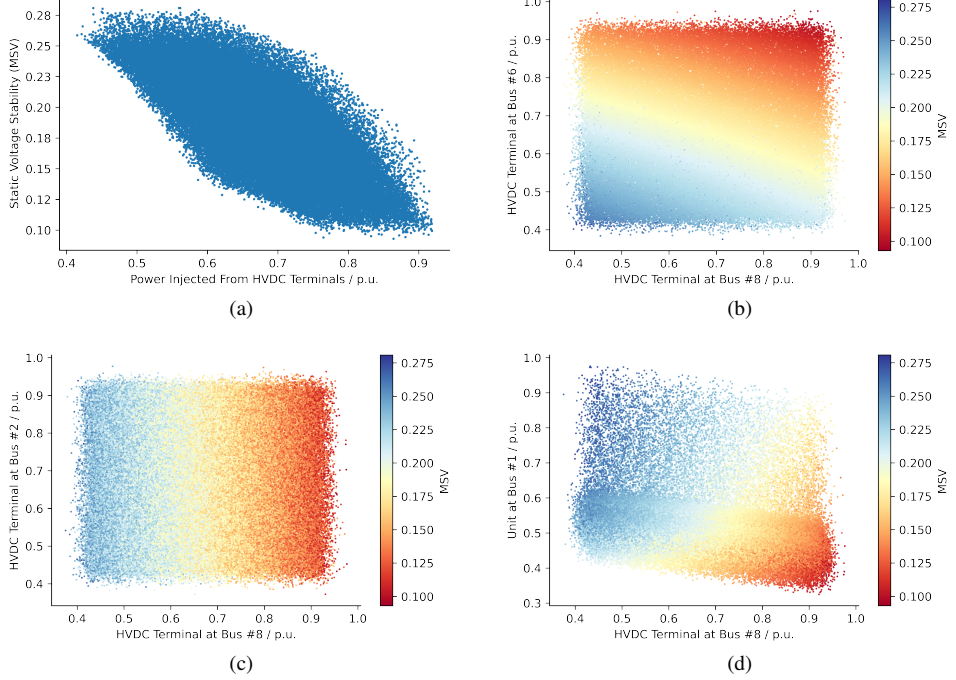


Fig. 5. Relationship between the voltage stability margin and Unit/HVDC outputs (IEEE-14 case).

TABLE I
STATISTIC INDICES FOR THE EXTRACTION

Accuracy	Recall	Precision	F1 Score
0.97	0.99	0.97	0.99

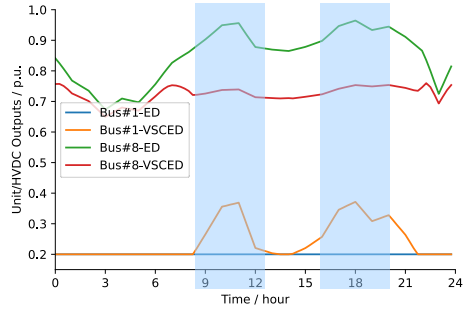


Fig. 6. Scheduling results on IEEE-14 case.

C. VSCED Model Performance

This subsection studies the effect of the voltage stability rule on economic dispatch problems based on the Jiangsu-2020 case. Four related numerical experiments are settled to study the proposed model's performance. For convenience, we use italic capital letter *A-D* to represent the following four models: *A* represents the ED without any voltage stability constraint, which acts as a benchmark; *B* represents the VSCED embedded with the linear rule; *C* represents the VSCED embedded with the quadratic dense rule; *D* represents the VSCED embedded with the quadratic sparse rule. Among these models, *D* is our proposed VSCED model. Table II shows the performance of the four models in the Jiangsu-2020

case.

Firstly, regarding the computation time of ED problems, the data suggests that the solving time of the proposed model is close to that of the benchmark and is acceptable. The benchmark model *A* takes 0.78 seconds. Model *B* takes 1.09 seconds, which is 39.7% longer than the benchmark. Model *C* takes too long to converge into the optimum. Our proposed model *D* takes 1.22 seconds, which is 69.2% longer than what the benchmark takes and is 11.9% longer than that *B* takes. Fig. 7 illustrates the comparison of the sparsity patterns of the quadratic rule coefficient matrix *A*. Fig. 7(a) shows the sparsity pattern of the rule extracted from the standard SVM, which is used in model *C*. This rule seems to be dense. However, if we set its entries less than 1×10^{-6} to zero, the sparsity pattern will be much more sparse, as shown in Fig. 7(b). Suppose these entries are not set to zero. In that case, the number of decision variables will increase, and the numerical conditions of the optimization problem (VSCED) will also deteriorate severely, making the VSCED difficult to solve. The proposed S-SVM in this paper can induce sparse rules while controlling the loss of accuracy and thus may effectively address this issue. Fig. 7(c) shows the sparsity pattern of the rule extracted from the proposed S-SVM, which is used in model *D*. It suggests that the proposed method greatly improves the sparsity of the quadratic coefficient matrix *A* and thus reduces the dimension of the introduced decision matrix *X*. This result is consistent with the time consumption results of Table II since the time complexity for the SDP model is greatly influenced by the dimension of the introduced decision matrix *X*. As stated above, the numerical results show that the proposed methods are computational tractable for practical power systems.

Another important comparison lies in the pass rate of the

TABLE II
MODEL PERFORMANCE COMPARISON

Case	Performance	<i>A</i> ¹	<i>B</i> ²	<i>C</i> ³	<i>D</i> ⁴
IEEE-14	Time / s	0.081	0.089	0.173	0.102
	Cost / M\$	6.7297	6.7313	6.7311	6.7312
	Pass Rate / %	35.42	81.25	92.71	100.00
Jiangsu	Time / s	0.78	1.09	over 600	1.22
	Cost / M\$	135.66	135.67	—	135.69
	Pass Rate / %	39.58	42.71	—	100.00

¹ ED

² Linear rule VSCED

³ Quadratic dense rule VSCED

⁴ Quadratic sparse rule VSCED

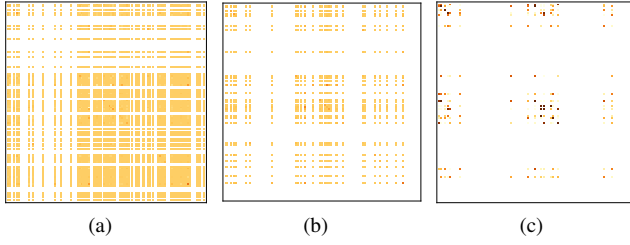


Fig. 7. Sparsity pattern of matrix *A*. (a) Original sparsity pattern corresponding to the dense rule (model *C*). (b) Sparsity pattern with entries less than 1×10^{-6} set to zero (approximated model *C*). (c) Sparsity pattern of the sparse rule (model *D*).

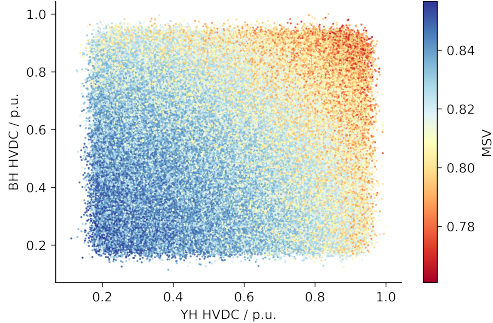


Fig. 8. Nonlinear voltage stability boundary. Here only shows the two-dimensional projection (Jiangsu-2020 case).

voltage stability margin. The pass rate is defined as the rate of the number of operation points with a sufficient voltage stability margin. Fig. 9 shows detailed voltage stability margins of the scheduling results. The blue cross represents the scheduling results of the benchmark ED; the orange/green point represents the scheduling results of VSced (with the linear/quadratic voltage stability constraint). The black dot line represents the required voltage stability margin, and any operation point below this line faces a voltage stability issue. It suggests that the linear rule is sometimes invalid, which is consistent with the nonlinear voltage stability boundary, as Fig. 8 shows. This figure also suggests that the voltage stability boundary is close to the quadratic boundary, which supports the proposed model from another angle.

Finally, we compare the scheduling results for the four ultra HVDC terminals. Fig. 10 compares the scheduling results of ED (model *A*) and VSced (model *D*). The results suggest that

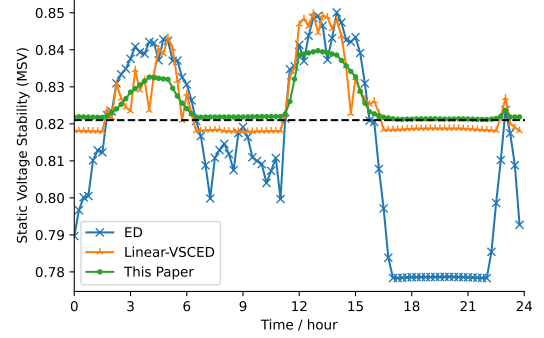


Fig. 9. Voltage stability comparison between ED and VSced on Jiangsu-2020 case. The black dot line represents the required voltage stability margin, and any operation point below this line faces a voltage stability issue.

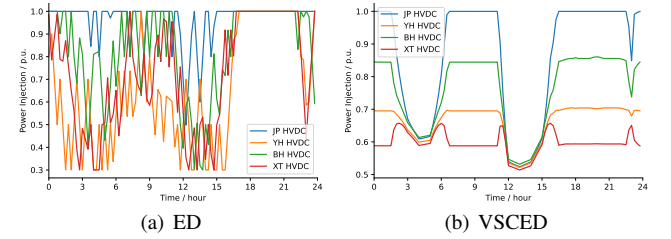


Fig. 10. Scheduling results comparison (Jiangsu-2020 case).

1) Without voltage stability constants, outputs of the HVDC terminals are excessively scheduled during peak load periods (7:00-11:00 and 17:00-22:00), which introduces a risk to the power system's voltage stability. 2) With voltage stability constraints, outputs of the HVDC terminals are scheduled within a secure range, which reserves the required voltage stability margin for the system. 3) Different HVDC terminals are limited under different levels according to their influence on voltage stability. Therefore, the results mentioned above explain how the VSced model behaves.

D. Comparison With Decision Tree and Multilayer Perceptron

In this subsection, the other two typical data-driven methods, decision tree (DT) and multilayer perceptron (MLP), are compared with our proposed method based on the Jiangsu-2020 system. The basic Jiangsu-2020 ED model is set to be the same, but the results of DT or MLP replace the voltage stability rule. Both the two VSced models are formulated as mixed integer linear programming (MILP), and the modeling details can be found in Appendix. For convenience, we use DT-VSced to refer to ED embedded with DT rules and MLP-VSced to refer to ED embedded with MLP rules.

A DT model with a depth of 7 is used in this paper as a comparison. The number of the positive leaves is $n_s = 52$. Therefore, the number of the required binary decision variables is $n_s T = 4992$. An MLP model with three layers (including the input and output layers) is also used as a comparison. The number of all the neurons is $n_s = 24$. Therefore, the number of the required binary decision variables is $n_s T = 2304$.

The results of the abovementioned models are shown in Fig. 11 and in Table III. In terms of computation time, both

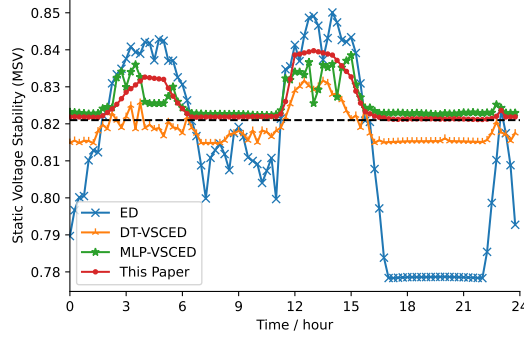


Fig. 11. Comparison of voltage stability margins under different data-driven methods on Jiangsu-2020 case. The black dot line represents the required voltage stability margin, and any operation point below this line faces a voltage stability issue.

TABLE III
COMPARISON WITH OTHER DATA-DRIVEN METHODS

	DT	MLP	This paper ¹
Binary Variables	4992	2304	0
Time	48.10 min	65.87 min	1.22 sec
Cost / M\$	135.78	135.82	135.69
Pass Rate / %	22.92	100.00	100.00

¹ i.e., model D in last subsection.

DT-VSCED and MLP-VSCED require more computing time. It takes 48.10 minutes to solve DT-VSCED, which is 2365 times the computing cost of our proposed model. It takes 65.87 minutes to solve DT-VSCED, which is 3239 times the computing cost of our proposed model. Such a large time difference between DT-VSCED/MLP-VSCED and our proposed model mainly comes from the introduction of binary variables. Although the depth of DT and the total neuron number of MLP are carefully set as small as possible, the computation time of solving such MILP problems is still high, especially when considering multiple time horizons. In addition, the introduced mixed integer constraints' structure also influences the computation time. Although the number of the introduced binary decision variables of MLP-VSCED is less than that of DT-VSCED, the computation time of MLP-VSCED is slightly higher than that of DT-VSCED. One possible reason for the above result is that the constraints extracted from DT are sparse with respect to the state variables (see Appendix). In terms of pass rate, both MLP-VSCED and our proposed model improve the pass rate to 100%, while the improvement of DT-VSCED is not significant. The pass rate results suggest that a DT with a deeper depth may be required to extract the voltage stability rule more precisely for the Jiangsu-2020 case. However, since the computation time of DT-VSCED grows exponentially as the depth increases, the DT with the depth of 7 used here is sufficient to be a comparison case. In addition, after some other tests, the number of neurons cannot be reduced anymore; otherwise, the performance will deteriorate.

Therefore, the above comparison suggests that our proposed model performs well in computation time and improvement effect.

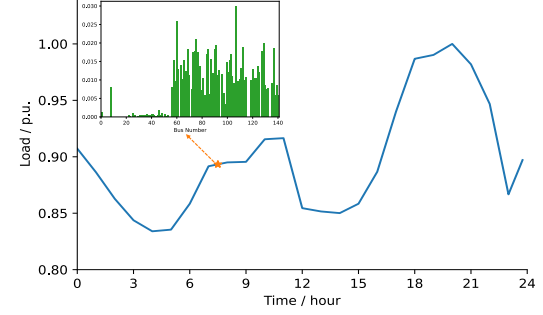


Fig. 12. Baseline load profile for Jiangsu-2020 case. The blue curve represents the temporal variation of the overall load demand in the system; the green bar chart illustrates the distribution of the load demand across different buses in the system at a specific time.

E. Generalization to Different Load Levels

The proposed VSCED model's generalization to different load levels is studied in this subsection. The baseline load curve is shown in Fig. 12, which is the same as the one used in Section IV-C to IV-D. We generate five more load curves by applying a scaling factor Δ to the baseline load curve as

$$\tilde{d}_t = (100\% + \Delta) \times d_t, \quad \forall t \in \mathcal{T}, \quad (28)$$

where $\Delta \in \{0\%, 1\%, 2\%, 3\%, 4\%, 5\%\}$ simulates the load growth rate in reality. Especially, $\Delta = 0\%$ represents the baseline load curve. We solved the corresponding ED and VSCED models for each loading scenario. The voltage stability rules used in all these VSCED models are the same as the ones used in Section IV-C. The scheduling results for each scenario are shown in Fig. 13.

Within an acceptable range of load level variation, the proposed VSCED model exhibits good generalization ability to the load level. From Fig. 13, it can be observed that the static voltage stability margin tends to decrease as the system load increases. However, despite the increment in the load level, the proposed voltage stability rules still effectively constrain the VSCED model. In all these scenarios, the VSCED model achieved the target of reserving voltage stability margins above the required threshold, ensuring that the system scheduling results reserve sufficient voltage stability margins.

However, it should be noted that updating the dataset and retraining the voltage stability rules are required when the load or other parameters change significantly. For example, it is unreasonable to expect a rule trained on summer data to apply to economic dispatch in the winter. Therefore, updating the dataset and retraining the voltage stability rules are strongly recommended when the condition of the future operating scenarios changes.

V. CONCLUSION

This paper built a VSCED model for multi-infeed LCC-HVDC power systems. Firstly, S-SVM is proposed to extract the nonlinear static voltage stability rule. Then a semi-definite reformulation method is applied to the extracted voltage stability rule. Finally, the rule is embedded into ED based on the reformulation without introducing any integer decision

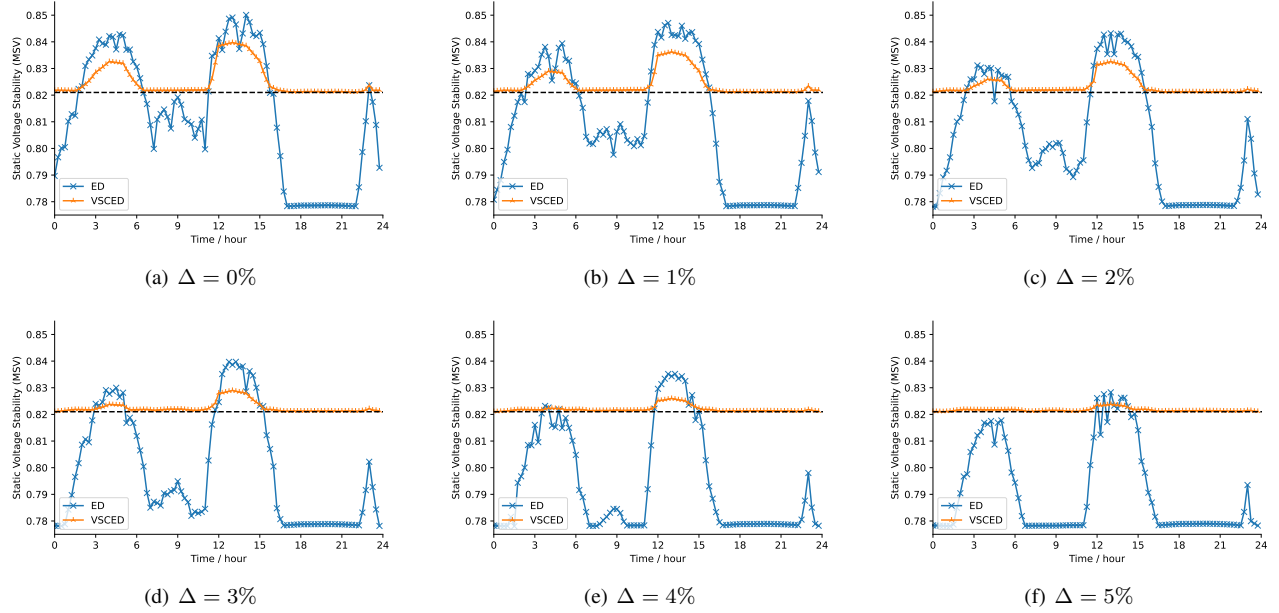


Fig. 13. Generalization to different load levels on Jiangsu-2020 case. The black dot line represents the required voltage stability margin, and any operation point below this line faces a voltage stability issue.

variable. The complete VSCED is then modeled as an SDP problem. The case studies based on a modified IEEE-14 system and a real-world Jiangsu system validated the effect and efficiency of the VSCED model. The results suggest that 1) the solving time, which is a little longer than that of ED, is acceptable. 2) The voltage stability margins are reserved above the required threshold at a small economic cost.

The proposed model is not restricted to economic dispatch, it can be further applied to other optimizations in power systems, such as voltage stability constrained unit commitment. Moreover, the result of the voltage stability rule can also give instructions to plan the position and quantity of the compensators to maintain the voltage stability.

APPENDIX REFORMULATIONS FOR TYPICAL DATA-DRIVEN MODELS

A. Decision Tree

The decision process of a decision tree (DT) consists of many parallel linear rule sequences. Each linear rule sequence corresponds to a unique path from a leaf node to the root node. Let d be the depth of a DT, n_s be the number of leaves representing stable labels, and n be the number of features. Then the extracted stability rule by DT can be expressed as

$$\begin{aligned} A^{(1)}\mathbf{x} - \mathbf{b}^{(1)} &\leq 0 & \text{or} \\ A^{(2)}\mathbf{x} - \mathbf{b}^{(2)} &\leq 0 & \text{or} \\ &\vdots \\ A^{(n_s-1)}\mathbf{x} - \mathbf{b}^{(n_s-1)} &\leq 0 & \text{or} \\ A^{(n_s)}\mathbf{x} - \mathbf{b}^{(n_s)} &\leq 0 \end{aligned} \quad (29)$$

where $A^{(k)} \in \mathbb{R}^{d \times n}$, $\mathbf{b}^{(k)} \in \mathbb{R}^d$ ($k = 1, 2, \dots, n_s$) represents the collection of the coefficients along the k th path (each row of $A^{(k)}$ involves only one state variable). To model the

OR relationship in optimization, binary decision variables are required. The stability constraints are reformulated as follows.

$$\left\{ \begin{array}{l} (\mathbf{x}, z) \in \mathbb{R}^n \times \{0, 1\}^{n_s} \\ \left. \begin{array}{l} A^{(1)}\mathbf{x} - \mathbf{b}^{(1)} \leq M(1 - z_1) \\ A^{(2)}\mathbf{x} - \mathbf{b}^{(2)} \leq M(1 - z_2) \\ \vdots \\ A^{(n_s)}\mathbf{x} - \mathbf{b}^{(n_s)} \leq M(1 - z_{n_s}) \\ \mathbf{1}^\top \mathbf{z} \geq 1 \end{array} \right. \end{array} \right\} \quad (30)$$

where $M > 0$ is large enough. Also, different z_t should be introduced for different time horizons t .

It should be noted that the number of stable leaves n_s has an inherent relationship with the depth d . For a balanced DT, the number of all leaves equals 2^d , thus $n_s \approx 2^{d-1}$. From this relationship, we see that the number of introduced binary decision variables increases exponentially with the depth of DT, which also represents its fitting ability.

B. Multilayer Perceptron

Multilayer perceptron (MLP) is a typical neural network. The structure of MLP consists of linear layers and active layers. Usually, the ReLu function $\max\{\cdot, 0\}$ is used as the active layers. Let n_l be the number of layers (every layer consists of one linear layer and one active layer), d_k be the input dimension of the k th layer, and $W^{(k)} \in \mathbb{R}^{d_{k+1} \times d_k}$, $\mathbf{b}^{(k)} \in \mathbb{R}^{d_{k+1}}$ be the coefficients of the k th layer ($d_{n_l+1} = 1$). Then, the

extracted stability rule by MLP can be expressed as

$$\begin{aligned} \mathbf{y}^{(1)} &= \max\{W^{(1)}\mathbf{x} + \mathbf{b}^{(1)}, 0\} \\ \mathbf{y}^{(2)} &= \max\{W^{(2)}\mathbf{y}^{(1)} + \mathbf{b}^{(2)}, 0\} \\ &\vdots \\ \mathbf{y}^{(n_l-1)} &= \max\{W^{(n_l-1)}\mathbf{y}^{(n_l-2)} + \mathbf{b}^{(n_l-1)}, 0\} \\ \mathbf{y}^{(n_l)} &= \max\{W^{(n_l)}\mathbf{y}^{(n_l-1)} + \mathbf{b}^{(n_l)}, 0\} \\ \mathbf{y}^{(n_l)} &\geq 0.5 \end{aligned} \quad (31)$$

where we assume $\mathbf{y}^{(n_l)} \geq 0.5$ represents that the stability margin satisfies the requirement. To model the ReLu active function $\max\{\cdot, 0\}$ in optimization, binary decision variables are required. The stability constraints are reformulated as follows.

$$\left\{ \begin{array}{l} (\mathbf{x}, \mathbf{z}) \mid \begin{array}{l} \mathbf{y}^{(0)} = \mathbf{x} \in \mathbb{R}^n \\ \mathbf{y}^{(k)} \geq W^{(k)}\mathbf{y}^{(k-1)} + \mathbf{b}^{(k)} \\ \mathbf{y}^{(k)} \leq W^{(k)}\mathbf{y}^{(k-1)} + \mathbf{b}^{(k)} + M(\mathbf{1} - \mathbf{z}^{(k)}) \\ \mathbf{y}^{(k)} \leq M\mathbf{z}^{(k)} \\ \mathbf{y}^{(k)} \geq 0 \\ \mathbf{z}^{(k)} \in \{0, 1\}^{d_{k+1}} \\ k = 1, 2, \dots, n_l \\ \mathbf{y}^{(n_l)} \geq 0.5 \end{array} \end{array} \right\} \quad (32)$$

where $M > 0$ is large enough. It is easy to see that the number of introduced binary decision variables equals the number of neurons. Also, different \mathbf{z}_t should also be introduced for different time horizons t .

REFERENCES

- [1] F. Zhang, H. Xin, D. Wu, Z. Wang, and D. Gan, "Assessing strength of multi-infeed lcc-hvdc systems using generalized short-circuit ratio," *IEEE Transactions on Power Systems*, vol. 34, no. 1, pp. 467–480, 2019.
- [2] L. Pengfei, "Research on hvdc operation characteristics under influence of hybrid ac/dc power grids," *Power System Technology*, vol. 46, no. 2, pp. 503–510, 2022.
- [3] B. Kroposki, B. Johnson, Y. Zhang, V. Gevorgian, P. Denholm, B.-M. Hodge, and B. Hannegan, "Achieving a 100% renewable grid: Operating electric power systems with extremely high levels of variable renewable energy," *IEEE Power and energy magazine*, vol. 15, no. 2, pp. 61–73, 2017.
- [4] Q. Hou, E. Du, N. Zhang, and C. Kang, "Impact of high renewable penetration on the power system operation mode: A data-driven approach," *IEEE Transactions on Power Systems*, vol. 35, no. 1, pp. 731–741, 2019.
- [5] C. Wang, B. Cui, Z. Wang, and C. Gu, "SDP-Based Optimal Power Flow With Steady-State Voltage Stability Constraints," *IEEE Transactions on Smart Grid*, vol. 10, no. 4, pp. 4637–4647, Jul. 2019. [Online]. Available: <https://ieeexplore.ieee.org/document/8439024/>
- [6] M. Nojavan and H. Seyed, "Voltage Stability Constrained OPF in Multi-Micro-Grid Considering Demand Response Programs," *IEEE Systems Journal*, vol. 14, no. 4, pp. 5221–5228, Dec. 2020. [Online]. Available: <https://ieeexplore.ieee.org/document/8960513/>
- [7] Z. Chu and F. Teng, "Short circuit current constrained uc in high ibg-penetrated power systems," *IEEE Transactions on Power Systems*, vol. 36, no. 4, pp. 3776–3785, 2021.
- [8] J. Liu, Z. Yang, J. Zhao, J. Yu, B. Tan, and L. Wenyuan, "Explicit data-driven small-signal stability constrained optimal power flow," *IEEE Transactions on Power Systems*, pp. 1–1, 2021.
- [9] M. S. S. Danish, T. Senju, S. M. S. Danish, N. R. Sabory, N. K., and P. Mandal, "A recap of voltage stability indices in the past three decades," *Energies*, vol. 12, no. 8, 2019. [Online]. Available: <https://www.mdpi.com/1996-1073/12/8/1544>
- [10] H. Xiao, Y. Li, D. Shi, J. Chen, and X. Duan, "Evaluation of strength measure for static voltage stability analysis of hybrid multi-infeed dc systems," *IEEE Transactions on Power Delivery*, vol. 34, no. 3, pp. 879–890, 2019.
- [11] M. M. Bhaskar, M. Srinivas, and S. Maheswarapu, "Security constraint optimal power flow(scopf)- a comprehensive survey," *Global Journal of Technology and Optimization*, vol. 2, no. 11, 2011.
- [12] M. Anghel, F. Milano, and A. Papachristodoulou, "Algorithmic construction of lyapunov functions for power system stability analysis," *IEEE Transactions on Circuits and Systems I: Regular Papers*, vol. 60, no. 9, pp. 2533–2546, 2013.
- [13] P. Kessel and H. Glavitsch, "Estimating the voltage stability of a power system," *IEEE Transactions on power delivery*, vol. 1, no. 3, pp. 346–354, 1986.
- [14] V. Ajjarapu and C. Christy, "The continuation power flow: a tool for steady state voltage stability analysis," *IEEE Transactions on Power Systems*, vol. 7, no. 1, pp. 416–423, 1992.
- [15] V. S. S. Kumar, K. K. Reddy, and D. Thukaram, "Coordination of reactive power in grid-connected wind farms for voltage stability enhancement," *IEEE Transactions on Power Systems*, vol. 29, no. 5, pp. 2381–2390, 2014.
- [16] M. Mokari and M. H. Moradi, "Security constraint optimal reactive power dispatch under uncertainty in a wind integrated power system," in *2020 55th International Universities Power Engineering Conference (UPEC)*. IEEE, 2020, Conference Proceedings, pp. 1–6.
- [17] F. Milano, C. A. Canizares, and A. J. Conejo, "Sensitivity-based security-constrained opf market clearing model," *IEEE Transactions on Power Systems*, vol. 20, no. 4, pp. 2051–2060, 2005.
- [18] Z. Wang, B. Cui, and J. Wang, "A necessary condition for power flow insolvability in power distribution systems with distributed generators," *IEEE Transactions on Power Systems*, vol. 32, no. 2, pp. 1440–1450, 2017.
- [19] B. Cui and X. A. Sun, "A new voltage stability-constrained optimal power-flow model: Sufficient condition, socp representation, and relaxation," *IEEE Transactions on Power Systems*, vol. 33, no. 5, pp. 5092–5102, 2018.
- [20] L. Duchesne, E. Karangelos, and L. Wehenkel, "Recent developments in machine learning for energy systems reliability management," *Proceedings of the IEEE*, vol. 108, no. 9, pp. 1656–1676, 2020.
- [21] Y. Luo, C. Lu, L. Zhu, and J. Song, "Data-driven short-term voltage stability assessment based on spatial-temporal graph convolutional network," *International Journal of Electrical Power & Energy Systems*, vol. 130, p. 106753, Sep. 2021. [Online]. Available: <https://linkinghub.elsevier.com/retrieve/pii/S0142061520342988>
- [22] Y. Seyed, H. Karimi, and J. Mahseredjian, "A Data-Driven Method for Prediction of Post-Fault Voltage Stability in Hybrid AC/DC Microgrids," *IEEE Transactions on Power Systems*, pp. 1–1, 2022. [Online]. Available: <https://ieeexplore.ieee.org/document/9677991/>
- [23] M. Cui, F. F. Li, H. Cui, S. Bu, and D. Shi, "Data-Driven Joint Voltage Stability Assessment Considering Load Uncertainty: A Variational Bayes Inference Integrated with Multi-CNNs," *IEEE Transactions on Power Systems*, pp. 1–1, 2021. [Online]. Available: <https://ieeexplore.ieee.org/document/9536417/>
- [24] Z. Zhang, E. Du, F. Teng, N. Zhang, and C. Kang, "Modeling Frequency Dynamics in Unit Commitment With a High Share of Renewable Energy," *IEEE Transactions on Power Systems*, vol. 35, no. 6, pp. 4383–4395, Nov. 2020. [Online]. Available: <https://ieeexplore.ieee.org/document/9099053/>
- [25] Z. Zhang, E. Du, G. Zhu, N. Zhang, C. Kang, M. Qian, and J. P. S. Catalão, "Modeling frequency response dynamics in power system scheduling," *Electric Power Systems Research*, vol. 189, p. 106549, Dec. 2020. [Online]. Available: <https://www.sciencedirect.com/science/article/pii/S0378779620303539>
- [26] J. L. Cremer, I. Konstantelos, S. H. Tin demans, and G. Strbac, "Data-driven power system operation: Exploring the balance between cost and risk," *IEEE Transactions on Power Systems*, vol. 34, no. 1, pp. 791–801, 2019.
- [27] Q. Hou, N. Zhang, D. S. Kirschen, E. Du, Y. Cheng, and C. Kang, "Sparse oblique decision tree for power system security rules extraction and embedding," *IEEE Transactions on Power Systems*, vol. 36, no. 2, pp. 1605–1615, 2021.
- [28] A. Venzke, G. Qu, S. Low, and S. Chatzivasileiadis, "Learning optimal power flow: Worst-case guarantees for neural networks," in *2020 IEEE International Conference on Communications, Control, and Computing Technologies for Smart Grids (SmartGridComm)*, 2020, Conference Proceedings, pp. 1–7.
- [29] Y. Zhang, H. Cui, J. Liu, F. Qiu, T. Hong, R. Yao, and F. Li, "Encoding frequency constraints in preventive unit commitment using deep learning with region-of-interest active sampling," *IEEE Transactions on Power Systems*, vol. 37, no. 3, pp. 1942–1955, 2022.

- [30] R. M. Henriques, J. A. Passos Filho, and G. N. Taranto, "Determining voltage control areas in large scale power systems based on eigenanalysis of the qv sensitivity matrix," *IEEE Latin America Transactions*, vol. 19, no. 02, pp. 182–190, 2021.
- [31] H. Jiang, X. Dai, D. W. Gao, J. J. Zhang, Y. Zhang, and E. Muljadi, "Spatial-temporal synchrophasor data characterization and analytics in smart grid fault detection, identification, and impact causal analysis," *IEEE Transactions on Smart Grid*, vol. 7, no. 5, pp. 2525–2536, 2016.
- [32] F. Zhang, H. Xin, Z. Wang, D. Gan, Q. Xu, P. Dai, and F. Liu, "Generalized short circuit ratio for multi-infeed lcc-hvdc systems," in *2017 IEEE Power Energy Society General Meeting*, 2017, pp. 1–5.
- [33] G. W. Stewart, *Matrix perturbation theory*. Citeseer, 1990, pp. 114–134.
- [34] F. Thams, A. Venzke, R. Eriksson, and S. Chatzivasileiadis, "Efficient database generation for data-driven security assessment of power systems," *IEEE Transactions on Power Systems*, vol. 35, no. 1, pp. 30–41, 2020.
- [35] J. Lan, Q. Guo, Y. Zhou, and H. Sun, "Generation of large-scale convergent power flow samples through a data-driven approach," in *IEEE 4th Conference on Energy Internet and Energy System Integration (EI2)*. IEEE, 2020, pp. 722–726.
- [36] S. Wu, W. Hu, Z. Lu, Y. Gu, B. Tian, and H. Li, "Power system flow adjustment and sample generation based on deep reinforcement learning," *Journal of Modern Power Systems and Clean Energy*, vol. 8, no. 6, pp. 1115–1127, 2020.
- [37] S. Boyd, S. P. Boyd, and L. Vandenberghe, *Convex optimization*. Cambridge university press, 2004.
- [38] A. Maher, "Semidefinite programming. methods and algorithms for energy management," Ph.D. dissertation, Université Paris Sud-Paris XI, 2013.



Hongyang Jia (S'20) received the B.S. degree in electrical engineering in 2021 from Tsinghua University, Beijing, China, where he is currently working toward the Ph.D. degree.

His research interests include renewable energy, power system operation and optimization, data driven power system analysis.



Ning Zhang (M'12–SM'18) received the B.S. and Ph.D. degrees from Tsinghua University, Beijing, China, in 2007 and 2012, respectively.

He is currently an Associate Professor with Tsinghua University. His research interests include power system planning and operation under renewable energy penetration, multiple energy systems integration.



Jiaxin Wang (S'21) received the B.S. degree in electrical engineering in 2022 from Tsinghua University, Beijing, China, where he is currently working toward the Ph.D. degree.

His research interests include power system operation and planning, renewable energy, optimization and machine learning.



Qingchun Hou (S'16) received the B.S. degree from Huazhong University of Science and Technology, Wuhan, China, in 2016, and the Ph.D. degree from Tsinghua University, Beijing, China, in 2021.

He is currently an algorithm expert with Alibaba. He was a recipient of the Advanced Technology Talent Program "AliStar" of Alibaba. His research interests include power system operation and planning with high renewable energy penetration, data-driven analytics, power system optimization, and machine learning.



Zhenyu Zhuo (S'17) received B.S. from the School of Electrical and Electronic Engineering in Huazhong University of Science and Technology, Wuhan, China in 2017. He received his Ph.D. degree from the Department of Electrical Engineering at Tsinghua University in 2022, working with Prof. Chongqing Kang.

His research interests include operations research, power system planning, renewable energy and low carbon power system technology.